COVID-19 impact on the concentration and composition of submicron particulate matter in a typical city of Northwest China

Jianzhong Xu[1*], Xinlei Ge[2*], Xinghua Zhang[1], Wenhui Zhao[1]

[1]State Key Laboratory of Cryospheric Science, Northwest Institute of Eco-Environment and Resources, Chinese Academy of Sciences, Lanzhou 730000, China

[2]Jiangsu Key Laboratory of Atmospheric Environment Monitoring and Pollution Control, Collaborative Innovation Center of Atmospheric Environment and Equipment Technology, School of Environmental Science and Engineering, Nanjing University of Information Science and Technology, Nanjing 210044, China

Corresponding author: Jianzhong Xu (jzxu@lzb.ac.cn) and Xinlei Ge (caxinra@163.com)

Key Points:

- The submicron aerosol loading was reduced by 40% during COVID-19 lockdown.
- The reduction of aerosol was mainly from secondary species due to reduction of primary precursors and low production rate.
- This result is contrast to that in East China where the aerosol loading was offset by secondary species production.

Abstract

In this study, we evaluated the variations of air quality in Lanzhou, a typical city in Northwestern China impacted by the COVID-19 lockdown. The mass concentration and chemical composition of non-refractory submicron particulate matter (NR-PM_1) were determined by a high-resolution aerosol mass spectrometry from January to March 2020. The concentration of NR-PM_1 dropped by 40% from pre- to during control period. The five aerosol components (sulfate, nitrate, ammonium, chloride, and organic aerosol (OA)) were all decreased during control period with the largest from secondary inorganic species (70% of the total reduction), whereas the OA sources did not vary synchronously. OA from coal and biomass burning remained stably from pre- to during control period, while traffic and cooking related emissions were reduced by 30% and 50%, respectively. The production rates for secondary inorganic and organic aerosols were also evaluated and represented a decreased trend from pre- to during control periods.

Plain Language Summary

At the beginning of 2020, a novel coronavirus disease (COVID-19) was spreading in China and lasting in the following two months. People's outdoor activities due to the coupling effect of this epidemic and Chinese New Year holiday were greatly reduced and pollutant emissions related with these activities were also reduced during this period. This situation provides us a unique chance to check on the air quality and evaluate the corresponding mitigation measures in the city. We observed a significant drop of the mass loading of NR-PM_1 by 40% in Lanzhou. The reduction of NR-PM_1 was mainly from secondary inorganic species accounting for 70% of reduced NR-PM_1. This finding is significantly different from that observed in Eastern China where the mass concentration of fine particulate matter was not reduced significantly with the reduction of primary emissions due to enhanced secondary production. The production rates for secondary inorganic and organic aerosols were also evaluated in our study and shown a decreased trend from pre- to during control period. These results may show a different situation on air pollution between East and West China.

1 Introduction

Lanzhou, locating in the northwest of China, is the capital of Gansu province and a typical city of northwestern China with coal combustion as the major fuel for residential heating during winter. Increased energy consumption and fast urbanization in past decades have aggravated its air pollution. In recent ten years, many great efforts have been conducted by the local government to improve the air quality and great achievement was reached (http://www.gov.cn/zwgk/2013-09/12/content_2486773.htm). Xu et al. (2016) presented an intensive study during wintertime in Lanzhou and demonstrated the improvement of air quality at this city comparing with its past. For Lanzhou, the chemical composition of non-refractory submicron particulate matter (NR-PM1) was mainly dominated by organic aerosol (OA, 51%), nitrate (17%) and sulfate (13%); the primary sources of OA included traffic emission, coal and biomass combustion, and cooking emission, while the secondary species were dominated by photochemical production.

During the winter of 2019, the same group conducted a study to monitor the spatial distribution of air pollutants of this city via the mobile measurement by using a suit of on-line instruments. Ten days before the Chinese New Year (CNY, January 25, 2020), the vehicle was stopped at the Yard of Northwest Institute of Eco-Environment and Resources, and to stationarity monitor the

air pollutants (Figure 1). The measurement lasted from January 14th to March 4th, 2020 which covered the periods of pre- and during the lockdown of Coronavirus Disease 2019 (COVID-19) pandemic (Tian et al., 2020). The life pattern of residents in this city as well as the primary emissions of air pollutants were greatly different from their normal states. This work provides a unique and timely investigation of the NR-PM_1 concentration and furthermore chemical composition, source contributions under different scenarios owing to the COVID-19 shutdown, therefore provide important implications into the control measures of air pollution in this and similar northwest Chinese cities.

2 Materials and Methods

The instruments placed inside the mobile truck included an Aerodyne high-resolution time-of-flight mass spectrometer (HR-ToF-AMS, Aerodyne, Inc., Billerica, MA, USA), a scanning mobility particle sizer (SMPS, model 3936, TSI Inc., Shoreview, MN, USA), and a carbon dioxide (CO_2) sensor (Model 840A, LICOR, USA). The inlet used a $PM_{2.5}$ cyclone to cut off the coarse PM. Before sampling by each instrument, the air flow was dried by a Nafion dyer, therefore the relative humidity was kept below 15% during the study. The HR-ToF-AMS was operated under only V-mode with 5 minutes resolution. The CO_2 recorded data at 1 second resolution, which were converted to 5 minutes resolution later for consistency.

All instruments were calibrated before sampling following standard methods. For example, the HR-ToF-AMS was calibrated for its flow rate, size, and ionization efficiency (IE) following the procedures described in Jayne et al. (2000); The IE calibration was conducted using NH_4NO_3 and $(NH_4)_2SO_4$ for ammonium and sulfate, respectively. The PAX was calibrated for its absorption and scattering using black carbon and ammonium sulfate, respectively; The CO_2 monitor was calibrated using with high-precision, high-accuracy CO_2 standard gas.

Data pre-processing was mainly conducted on HR-ToF-AMS data using the standard software, i.e., SQUIRREL (V1.63) and PIKA (V1.23) written in IGOR (Wavemetrics, Inc., Lake Oswego, OR, USA; http://cires.colorado.edu/jimenez-group/ToFAMSResources/ToFSoftware/index.html). An empirical particle collection efficiency (CE) of 0.5 was used, which was validated using composition-dependent CE included in software. These two CE results were highly consistent. Default relative ionization efficiency (RIE) values were used for organics (1.4), nitrate (1.1), and chloride (1.3), while an RIE value of 4.1 was determined for ammonium and 1.38 for sulfate based on the calibrations of pure NH_4NO_3 and $(NH_4)_2SO_4$, respectively. The source apportionment of OA was conducted by positive matrix factorization (PMF) with the robust engine. Six factors were identified including traffic emitted OA (HOA), biomass burning emitted OA (BBOA), coal combustion OA (CCOA), cooking-related OA (COA), low-oxidized oxygenated OA (LO-OOA), and more-oxidized

oxygenated OA (MO-OOA). Technical details can be found in our previous publications (Xu et al., 2014; Xu et al., 2016).

3 Results and Discussion

3.1 Variations of PM mass concentration pre- and during the COVID-19 lockdown period

Considering different life patterns during the COVID-19 lockdown, the sampling period was divided into four periods, i.e., normal period (P1, January 14th to January 23th, 2020), CNY holiday period (P2, January 24th to February 4th, 2020), strict control period (P3, February 5th to February 16th, 2020), and recovery period (P4, February 17th to March 4th, 2020). The life pattern in the city during P1 was basically normal, although many people prepared to leave for the CNY. During P2, many people left the city and people inside the city also reduced their outdoor activities; A portion of commercial stores also closed which reduced the fuel usage. During P3, with the increase of confirmed COVID-19 cases in China and Lanzhou, people were restricted to stay at home, therefore outdoor activities almost vanished, but instead the household activities could be enhanced during this period. For example, in order to maintain warm conditions in home, the usage of coal from communities and central heating plants would increase. During P4, with the decreased cases of COVID-19 and controlled pandemic, the government encouraged people to gradually return to work; Thus, the traffic and other anthropogenic activities gradually resumed. Overall, the P1 could be treated as a reference period with intense primary emissions, while these emissions during P2, P3, and P4 were all reduced but with different extents among them.

The meteorological data, chemical composition and mass concentration observed in this study were all shown in Figure 2. Note the data below were the arithmetic means value of each period. From P1 to P4, the wind conditions were quite stable with low wind speed (mean values: 1.5~1.6 m s^{-1}, Table 1) and dominating wind directions from eastern to northeastern (Figure 3). The average air temperature was increased step by step from –1.6 °C (P1) to 5.2 °C (P4) as well as for solar radiation (Table 1), while the relative humidity was continuously decreased from 52.5 ± 11.3% (P1) to 27.5 ± 14.6% (P4). Generally, these results indicated a warmer and dryer weather conditions transited from P1 to P4. The mass concentration of NR-PM_1 showed an evidently decreasing trend from P1 (36.4 μg m^{-3}) to P4 (15.8 μg m^{-3}) with a reduction rate of 40.1% from pre- (P1) to during pandemic (P2-P4) (Figure 3a). The mass concentration of NR-PM_1 during recovery period (P4) in Lanzhou did not increase, probably owing to the overall limited human activities and enhanced dispersion caused by higher plenary boundary layer heights. The similar trend was also observed by the environmental monitoring sites of Ministry of Ecology and Environment (MEE) in Lanzhou. There are total five sites including four urban sites and one background site (Figure 1). The observed mass loadings of air pollutants from these five sites are basically consistent (not shown). In this study, the results from Shengwusuo site that is closest to our sampling site was presented only (Figure 3f). The mass concentrations of $PM_{2.5}$ from this site during four periods were 52.3 ± 20.2 μg m^{-3}, 49.5 ± 17.4 μg m^{-3}, 36.4 ± 11.9 μg m^{-3}, and 33.8 ± 12.7 μg m^{-3}, respectively. The primary species of carbon monoxide (CO) also presented a decreased trend from P1 to P4 (1.6 ± 0.7 mg m^{-3} to 0.9 ± 0.5 g m^{-3}). Similar result was also observed for sulfur dioxide (SO_2) but the reduction was smaller (P1 to P4: 21.3 ± 7.3 to 17.0 ± 8.9 μg m^{-3}). Note the mass concentrations of PM_{10} decreased from P1 to P2 (86.1 ± 28.4 to 69.0

± 21.8 μg m^{-3}) but increased from P2 to P4 (102.4 ± 58.7 μg m^{-3}), likely due to influences of dust events.

The decreased PM concentration may closely be related with the reduction of primary emissions in these periods impacted by COVID-19 pandemic, but also potentially influenced by meteorological conditions. In order to eliminate the meteorological influences, a correction factor was calculated by comparing the concentration of CO at Shengwusuo site to that at the background site (Yuzhong) locating ~30 km downwind of Lanzhou (Figure 1). The air quality of Yuzhong was heavily influenced by the outflow of Lanzhou and the station is built on a mountaintop with little impacts from local emissions. The ratios of CO between these two stations could be treated as the diffusion rates of different periods. By normalizing to P1, the corrected factors were 1, 1.2, 1.2, and 1.12 for P1, P2, P3, and P4, respectively. The factor-corrected mass concentrations were shown in Figure 3b and the decreased trend was still distinct.

3.2 Variation of chemical composition and the sources during different periods

The chemical composition during four periods varied as well. During P1, NR-PM_1 was consisted of 44.6% OA, and important contributors of sulfate (17.7%), nitrate (21.0%), ammonium (12.4%), and chloride (4.4%), while the contributions of these species during P4 were 56.8% (OA), 10.5% (sulfate), 15.8% (nitrate), 10.0% (ammonium), and 6.9% (chloride), respectively. It is evident that the secondary inorganic species in total (sulfate, nitrate, chloride and ammonium) were decreased significantly from P1 to P4 with a reduction rate of 32.3 – 66.2%, accounting for 64.8 – 74.1% of the total reduction of NR-PM_1. The primary organic aerosol (POA, HOA + COA + BBOA + CCOA) also decreased from P1 to P4 with the mass loading of 9.7 μg m^{-3} at P1 to 6.3 μg m^{-3} at P4 with a reduction rate of 15 – 35% during P2 and P4. However, variations of these POA components were different from each other. COA decreased significantly from 2.9 to 1.2 μg m^{-3} (P1 to P2) but with slight increase from P3 to P4 (to ~1.6 μg m-3). The HOA decreased from P1 to P2 (2.0 to 1.2 μg m^{-3}) largely but slightly increased to 1.3 μg m^{-3} during P4. However, the loadings of BBOA and CCOA did not decrease, instead they increased during P2 and P3 (~0.4 μg m^{-3} for BBOA and ~0.1 μg m^{-3} for CCOA) than those during P1, but then decreased by ~1 μg m^{-3} for both species during P4. The secondary organic aerosol (SOA, LO-OOA + MO-OOA) concentration also declined from 6.5 (P1) to 2.6 μg m^{-3} (P4) with a reduction rate of 22.4 – 59.8% during P2 and P4. These results demonstrated that the reduction of NR-PM1 concentration was dominated by secondary species.

4 Discussion

Based on the results above, it is evident that the loading of PM during CNY and COVID-19 shutdown was reduced remarkably. The reduction rate of CO from P1 to P4 (43.8%) was comparable to the $PM_{2.5}$ (35.4%), but lower than that of NR-PM_1 (56.6%) as it was dominated by reduction of secondary species. The drop of secondary species from P1 to P2-P4 could be due to

the reduction of primary precursors and/or low production (or formation) rates. In this section, we further investigated the behaviors of both secondary inorganic and organic species.

4.1 Secondary inorganic aerosol species (SIA)

The production rates of sulfate and nitrate are evaluated through two ratios, i.e., SOR = $n\_{sulfate}/(n\_{SO2} + n\_{sulfate})$ and NOR = $n\_{nitrate}/(n\_{NO2} + n\_{nitrate})$ (Figure 4) (Xu et al., 2014). The data of SO_2 and NO_2 were taken from Shengwusuo site with one-hour resolution. These two ratios were found to continuously decrease from P1 to P4 with decrease rates between P1 and P2-P4 of 70% for sulfate and 37% for nitrate, respectively. In contrast to the variations of SO_2 and NO_2 (Figure 3f), the decreases of sulfate and nitrate production rates were more significant, indicating that the overall capacity of SO_2 and NO_2 oxidations decreased despite increased temperatures and decreased RH. The ratios of SOR and NOR also showed a positive relationship with primary emission tracer CO, especially at low concentration range, which indicate the formation of sulfate and nitrate were highly sensitive to variations of primary emissions. The atmospheric oxidants (such as hydroxyl radicals) in atmosphere are in large part depending upon photochemical processes involved with nitrogen oxides ($NOx = NO + NO_2$) and volatile organic compounds (VOCs) (Stein & Saylor, 2012), therefore reduction of these emissions may reduce its concentration therefore the oxidation capacity.

It should be noted that, our findings are in contrast with those observed in Eastern China. Huang et al. (2020) reports that the mass concentrations of $PM_{2.5}$ in Beijing, Tianjin and Hebei even slightly increased during COVID-19 lockdown and attributed to that production of secondary species offsets the reduction of primary emissions. Adverse meteorological conditions (Wang et al., 2020), such as low planetary boundary layer and calm wind, may further favor the secondary chemical processes under the conditions of enhanced atmospheric oxidation capacity.

4.2 Secondary organic aerosol species (SOA)

Similar to secondary inorganic species, we found that the SOA variation was also related with reduced emissions of its primary precursors and/or low production rate. We first checked on the relationship between POA and SOA and found a distinct positive correlation between them (R^2 = 0.8, Figure 5a), suggesting that the SOA reduction was closely associated with that of POA (some SOA might be products of further oxidation of POA). In this study, the most significant reduction of POA was from COA and HOA (mainly COA). This result suggests that cooking emission may be an important source of SOA in Lanzhou. Xu et al. (2016) suggested that non-fossil fuel combustion emission including cooking and biomass burning emissions was an important original source of SOA based on radiation carbon isotope analysis. Cooking emissions produce important precursors including alkenes, semi-volatile and intermediate-volatility organic compounds and are important sources of SOA in urban areas (Liu et al., 2018).

Moreover, the production of SOA is further investigated by using SOA versus CO_2 which can used as the production rate of aerosol per unit mass of fuel ($\Delta SOA/\Delta CO_2$) (Collier et al., 2016; Nault et al., 2018). It was found that the delta variations of SOA (slope of the fitting line) was one time lower during P3 and P4 than that of P1 (Figure 5b), suggesting a lower production rate of SOA during P3 and P4. The main types of precursors for SOA production could also be investigated by the scatter plot of SOA versus Ox ($O_3 + NO_2$) which are all products of

photochemical reactions (Herndon et al., 2008). High slopes between SOA and Ox suggest aromatic VOCs or oxidized VOCs dominated the photochemical processing, while low slopes were observed for alkene VOCs photochemical processing (Wood et al., 2010). Aromatic VOCs are important precursors of SOA formation with high reactivity and aerosol mass yields (Yuan et al., 2013; Ding et al., 2017; Peng et al., 2017). The slopes during four periods decreased from 0.073 (P1) to 0.023 (P4), suggesting the dominant SOA precursors changed with the CNY and COVID-19 lockdown, and the production rate of SOA significantly decreased likely due to this transition of precursors. Overall, the SOA behavior in Lanzhou during the CNY and COVID-19 is also different from that in Eastern China where the production rate of SOA was distinctly enhanced (Huang et al., 2020).

5 Conclusions

Mass concentrations and chemical compositions of NR-PM_1 during January to March 2020 were obtained in Lanzhou using a HR-ToF-AMS and used to analyze the variations of aerosol mass loadings and potential sources during the different stages of the COVID-19 impacted period. The results show that the mass concentration of NR-PM_1 dropped by 40% from pre- to control periods. This result was also supported by the data from MEE monitor stations in Lanzhou. Secondary inorganic components dominated the reduced mass loading (70%), whereas the contribution of OA from coal combustion and biomass burning mainly for industry and residential heating did not reduce. The reduction of cooking and traffic emission was on the other hand distinct during control period, and they might be sources of SOA therefore led to reduction of SOA concentration as well. We also found that the production rates of both secondary inorganic and organic aerosol components decreased during the control and recovery period, indicating a decrease of atmospheric oxidation capacity. Decrease of SOA production rate might be also associated with the change of its major precursors from highly reactive aromatics to other less reactive ones.

Overall, our findings here are in contrast with those observed in Eastern China, where oxidation capacity and production of secondary species were both enhanced and offset reduction of primary emissions and heavy haze could still occur during COVOD-19 lockdown. The strikingly different findings in Lanzhou, clearly manifest that the governing aerosol chemical processes in Northwest China are distinct from those in Eastern China. But on the other hand, it points out that strict control of primary emissions would be more effective in $PM_{2.5}$ alleviation in Lanzhou and other Northwestern cities than those in Eastern China.

Acknowledgments and Data Access

This research was supported by grants from the National Natural Science Foundation of China (41977189, 41771079, 41805106, and 41721091) and the Key Laboratory of Cryospheric Sciences Scientific Research Foundation (SKLCS-ZZ-2020). The data in this manuscript are available at https://zenodo.org/record/3855067#.Xs8BFDl5vmE.

References

Collier, S., S. Zhou, T. B. Onasch, D. A. Jaffe, L. Kleinman, A. J. Sedlacek, et al. (2016). Regional Influence of Aerosol Emissions from Wildfires Driven by Combustion

Efficiency: Insights from the BBOP Campaign, *Environ. Sci. Tech.*, *50*(16), 8613-8622, doi:10.1021/acs.est.6b01617.

Ding, X., Y.-Q. Zhang, Q.-F. He, Q.-Q. Yu, J.-Q. Wang, R.-Q. Shen, et al. (2017). Significant Increase of Aromatics-Derived Secondary Organic Aerosol during Fall to Winter in China, *Environ. Sci. Tech.*, *51*(13), 7432-7441, doi:10.1021/acs.est.6b06408.

Herndon, S. C., T. B. Onasch, E. C. Wood, J. H. Kroll, M. R. Canagaratna, J. T. Jayne, et al. (2008). Correlation of secondary organic aerosol with odd oxygen in Mexico City, *Geophys. Res. Lett.*, *35*(15), doi:10.1029/2008gl034058.

Huang, X., A. Ding, J. Gao, B. Zheng, D. Zhou, X. Qi, et al. (2020). Enhanced secondary pollution offset reduction of primary emissions during COVID-19 lockdown in China, *https://eartharxiv.org/hvuzy/*.

Jayne, J. T., D. C. Leard, X. Zhang, P. Davidovits, K. A. Smith, C. E. Kolb & D. R. Worsnop (2000). Development of an Aerosol Mass Spectrometer for Size and Composition Analysis of Submicron Particles, *Aerosol Sci. Tech.*, *33*(1-2), 49-70, doi:10.1080/027868200410840.

Liu, T., Z. Wang, D. D. Huang, X. Wang & C. K. Chan (2018). Significant Production of Secondary Organic Aerosol from Emissions of Heated Cooking Oils, *Environ. Sci. Tech. Lett.*, *5*(1), 32-37, doi:10.1021/acs.estlett.7b00530.

Nault, B. A., P. Campuzano-Jost, D. A. Day, J. C. Schroder, B. Anderson, A. J. Beyersdorf, et al. (2018). Secondary organic aerosol production from local emissions dominates the organic aerosol budget over Seoul, South Korea, during KORUS-AQ, *Atmos. Chem. Phys.*, *18*(24), 17769-17800, doi:10.5194/acp-18-17769-2018.

Peng, J., M. Hu, Z. Du, Y. Wang, J. Zheng, W. Zhang, et al. (2017). Gasoline aromatics: a critical determinant of urban secondary organic aerosol formation, *Atmos. Chem. Phys.*, *17*(17), 10743-10752, doi:10.5194/acp-17-10743-2017.

Stein, A. F. & R. D. Saylor (2012). Sensitivities of sulfate aerosol formation and oxidation pathways on the chemical mechanism employed in simulations, *Atmos. Chem. Phys.*, *12*(18), 8567-8574, doi:10.5194/acp-12-8567-2012.

Tian, H., Y. Liu, Y. Li, C.-H. Wu, B. Chen, M. U. G. Kraemer, et al. (2020). An investigation of transmission control measures during the first 50 days of the COVID-19 epidemic in China, *Science*, eabb6105, doi:10.1126/science.abb6105.

Wang, P., K. Chen, S. Zhu, P. Wang & H. Zhang (2020). Severe air pollution events not avoided by reduced anthropogenic activities during COVID-19 outbreak, *Resour. Conserv. Recycl.*, *158*, 104814, doi:10.1016/j.resconrec.2020.104814.

Wood, E. C., M. R. Canagaratna, S. C. Herndon, T. B. Onasch, C. E. Kolb, D. R. Worsnop, et al. (2010). Investigation of the correlation between odd oxygen and secondary organic aerosol in Mexico City and Houston, *Atmos. Chem. Phys.*, *10*(18), 8947-8968, doi:10.5194/acp-10-8947-2010.

Xu, J., J. Shi, Q. Zhang, X. Ge, F. Canonaco, A. S. H. Prévôt, et al. (2016). Wintertime organic and inorganic aerosols in Lanzhou, China: sources, processes, and comparison with the results during summer, *Atmos. Chem. Phys.*, *16*(23), 14937-14957, doi:10.5194/acp-16-14937-2016.

Xu, J., Q. Zhang, M. Chen, X. Ge, J. Ren & D. Qin (2014). Chemical composition, sources, and processes of urban aerosols during summertime in northwest China: insights from high-resolution aerosol mass spectrometry, *Atmos. Chem. Phys.*, *14*(23), 12593-12611, doi:10.5194/acp-14-12593-2014.

Yuan, B., W. W. Hu, M. Shao, M. Wang, W. T. Chen, S. H. Lu, et al. (2013). VOC emissions, evolutions and contributions to SOA formation at a receptor site in eastern China, *Atmos. Chem. Phys.*, *13*(17), 8815-8832, doi:10.5194/acp-13-8815-2013.

Figure 1. Location map of Lanzhou, our sampling site and five monitor sties of Minister of Ecology and Environment (MEE) network.

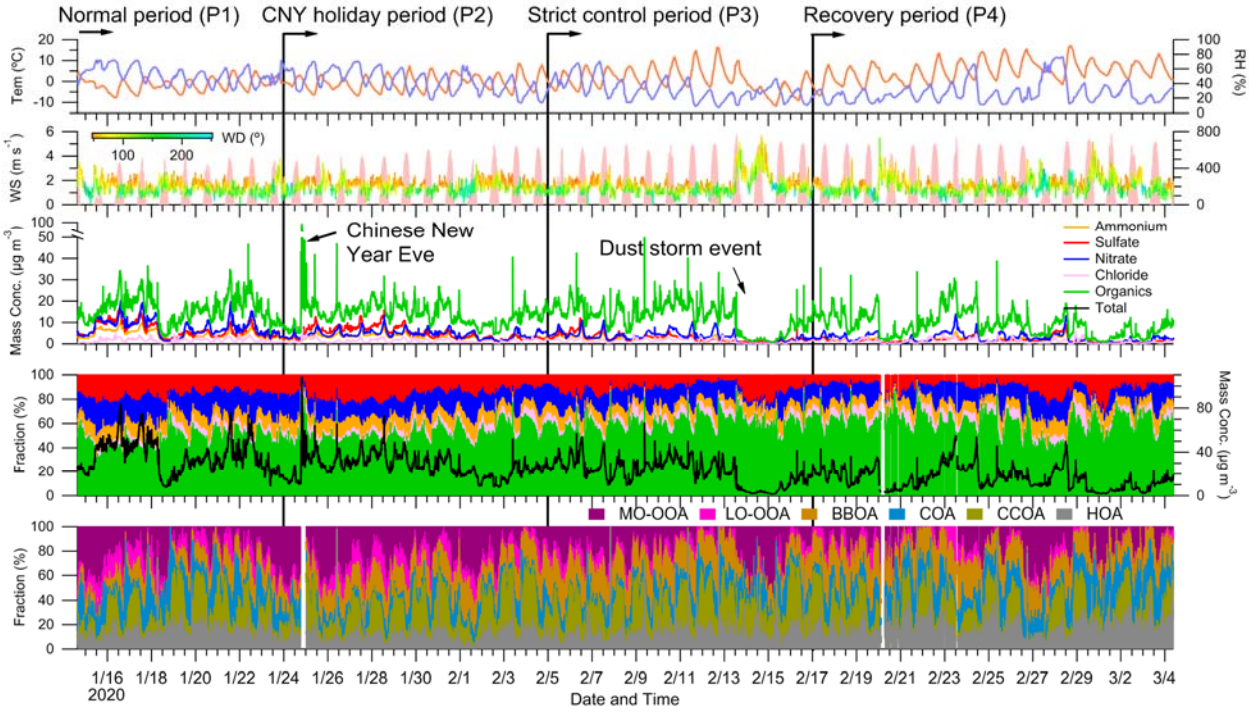

Figure 2. The combo plot of meteorological data and HR-ToF-AMS data.

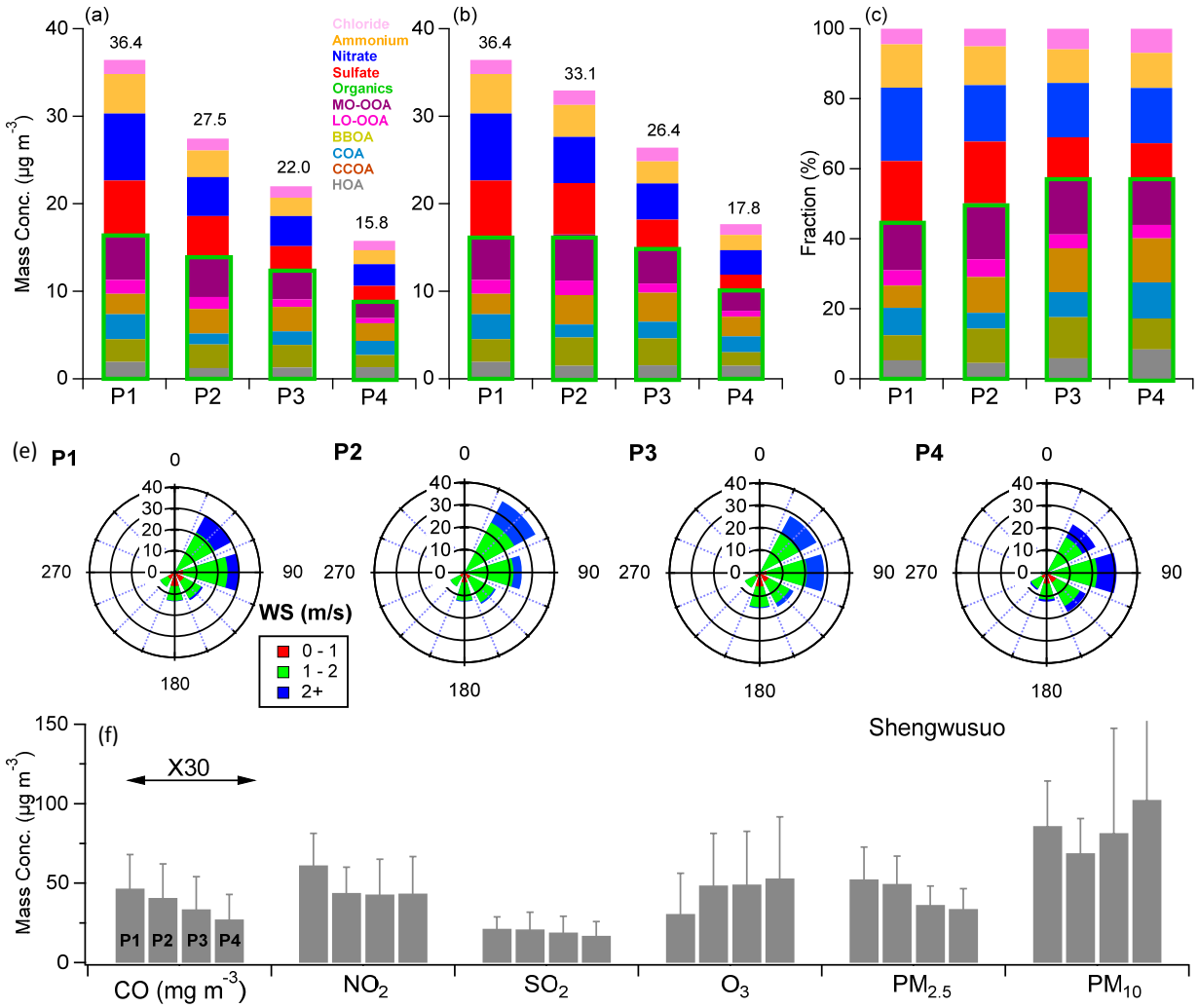

Figure 3. Comparison between four periods for (a, b, and c) mass concentration and chemical composition, (e) wind conditions, and (f) chemical species from MME network site of Shengwusuo.

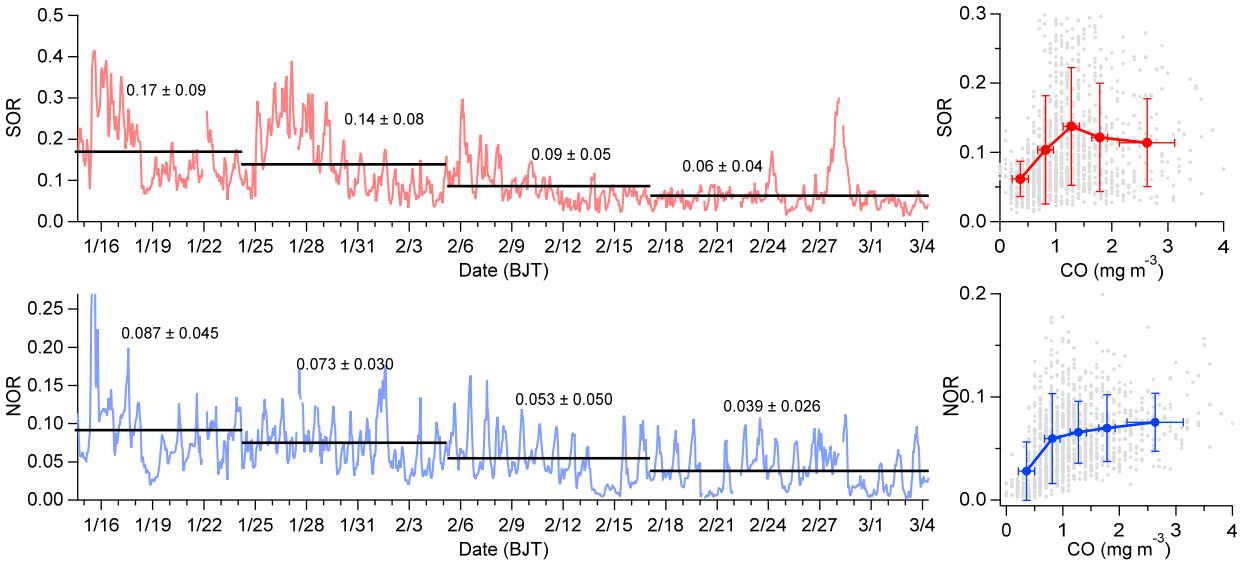

Figure 4. The production rate of sulfate and nitrate during four periods and relationship with primary species of carbon monoxide (CO). The production rate of SOR and NOR are defined as SOR = $n_{\_sulfate}/(n_{\_SO2} + n_{\_sulfate})$ and NOR = $n_{\_nitrate}/(n_{\_NO2} + n_{\_nitrate})$. SO_2 and NO_2 are from Shengwusuo site in Lanzhou.

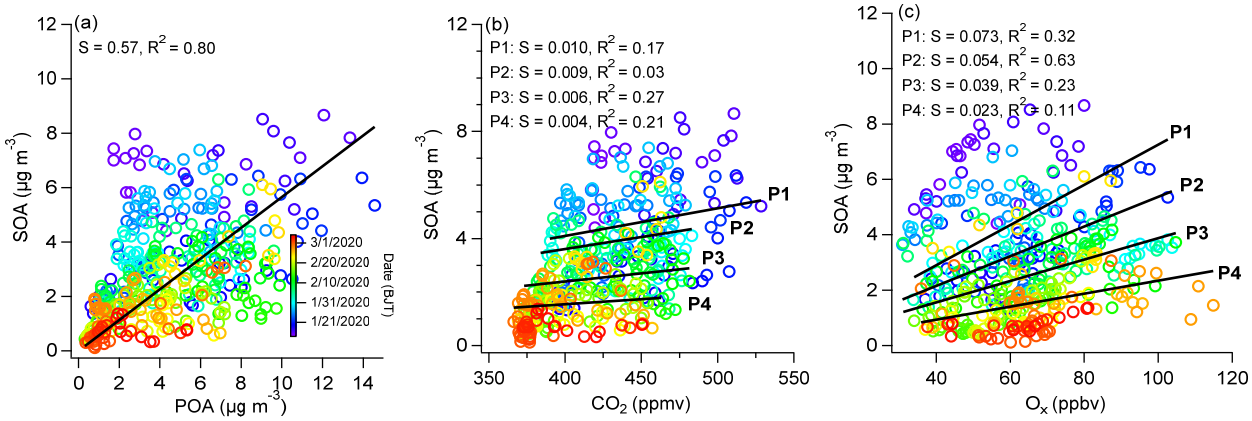

Figure 5. Scatter plots of (a) SOA vs. POA, (b) SOA vs. CO_2, and SOA vs. Ox (O_3 + NO_2). In (b) and (c), the linear fittings of the data during four periods were shown.

326 Table 1. The meteorological conditions during different periods.

	P1	P2	P3	P4
Wind speed (m s^{-1})	1.5 ± 0.53	1.5 ± 0.47	1.6 ± 0.78	1.6 ± 0.64
Air temperature (°C)	-1.6 ± 3.0	-0.5 ± 3.6	1.1 ± 5.4	5.2 ± 4.9
Relatively humidity (%)	52.5 ± 11.3	43.3 ± 15.0	31.0 ± 14.0	27.5 ± 14.6
Solar radiation (W m^{-2})	93.6 ± 154.1	127.6 ± 196.6	156.0 ± 230.3	162.4 ± 236.8
Sulfate	6.44 ± 3.26	4.84 ± 2.68	2.66 ± 1.89	1.66 ± 1.20
Nitrate	7.64 ± 3.92	4.42 ± 1.80	3.42 ± 2.34	2.49 ± 2.05
Chloride	1.62 ± 0.90	1.37 ± 0.81	1.29 ± 0.90	1.09 ± 0.95
Ammonium	4.50 ± 2.03	3.05 ± 1.17	2.12 ± 1.26	1.58 ± 1.03
HOA	1.95 ± 0.88	1.25 ± 0.77	1.29 ± 0.88	1.33 ± 0.73
COA	2.86 ± 2.05	1.24 ± 0.99	1.57 ± 1.11	1.63 ± 0.87
BBOA	2.31 ± 1.07	2.81 ± 0.70	2.77 ± 1.24	1.99 ± 0.82
CCOA	2.60 ± 1.98	2.69 ± 1.82	2.58 ± 1.48	1.39 ± 1.19
LO-OOA	1.58 ± 1.37	1.38 ± 0.99	0.86 ± 0.79	0.60 ± 0.69
MO-OOA	4.94 ± 2.61	4.39 ± 1.99	3.43 ± 2.16	2.02 ± 1.54
POA	9.72 ± 5.98	7.99 ± 4.28	8.21 ± 4.71	6.34 ± 3.61
SOA	6.52 ± 3.98	5.78 ± 2.98	4.29 ± 2.94	2.62 ± 2.23

327